SOIL, 11, 95–104, 2025
https://doi.org/10.5194/soil-11-95-2025

SOIL Open Access EGU

Organic pollutant oxidation on manganese oxides in soils – the role of calcite indicated by geoelectrical and chemical analyses

Sonya S. Altzitser, Yael G. Mishael, and Nimrod Schwartz

Department of Soil and Water Sciences, The Robert H. Smith Faculty of Agriculture, Food and Environment, The Hebrew University of Jerusalem, Rehovot, 7610001, Israel

Correspondence: Nimrod Schwartz (nimrod.schwartz@mail.huji.ac.il)

Received: 8 July 2024 – Discussion started: 22 August 2024
Revised: 10 November 2024 – Accepted: 26 November 2024 – Published: 28 January 2025

Abstract. Understanding phenolic-pollutant interactions with soil colloids has been a focus of extensive research, primarily under controlled conditions. This study addresses the need to explore these processes in a more natural, complex soil environment. We aim to shed light on the underlying mechanisms of hydroquinone (a representative phenolic pollutant) oxidation in ambient, MnO_2-rich sandy soil within soil columns designed for breakthrough experiments. Our innovative approach combines noninvasive electrical measurements, crystallographic and microscopic analyses, and chemical profiling to comprehensively understand soil–pollutant interactions. Our study reveals that hydroquinone oxidation by MnO_2 initiates a cascade of reactions, altering local pH, dissolving calcite, and precipitating amorphous Mn oxides, thereby showcasing a complex interplay of chemical processes. Our analysis, combining insights from chemistry and electrical measurements, reveals that the oxidation process led to a constant decrease in polarizing surfaces, as indicated by quadrature conductivity monitoring. Furthermore, dynamic shifts in the soil solution chemistry (changes in the calcium and manganese concentrations, pH, and electrical conductivity (EC)) correlated with the non-monotonous behavior of the in-phase conductivity. Our findings conclusively demonstrate that the noninvasive electrical method allows real-time monitoring of calcite dissolution, serving as a direct cursor to the oxidation process of hydroquinone and enabling the observation of chemical interactions in soil solution and on soil particle surfaces.

1 Introduction

Phenolic pollutants may originate from various sources, including agricultural, industrial, municipal, and medical wastes (Davì and Gnudi, 1999; Farhan Hanafi and Sapawe, 2020). Due to their chemical characteristics, phenolic pollutants tend to persist in soil and water at relatively low concentrations for an extended period, posing a significant environmental threat. The chemical fate of these pollutants in soil has been extensively studied, with particular attention given to processes such as adsorption–desorption and oxidation (Ahmed et al., 2015; Delgado-Moreno et al., 2021; Kang and Choi, 2008; Lambert, 2018; Loffredo and Senesi, 2006; Sun et al., 2022). With regard to oxidation, various oxides, both natural and engineered, have been investigated for their potential to remove phenolic pollutants (Gusain et al., 2019; Remucal and Ginder-Vogel, 2014). Among these, birnessite (MnO_2), a manganese oxide naturally found in soils, is known for its effectiveness in oxidizing various phenolic compounds (Murray, 1974; Remucal and Ginder-Vogel, 2014).

While manganese oxides' abilities to oxidize phenols have been explored widely, most of these studies have been conducted in buffered, controlled environments within batch experiments, which may not accurately reflect manganese oxide behavior in more complex, heterogeneous soil (Chien et al., 2009; Fukuzumi et al., 1975; Liao et al., 2021; Liu et al., 2011; McBride, 1987; McKenzie, 1971; Shindo and Huang, 1984; Stone and Ulrich, 1989; Trainer et al., 2021). To the best of our knowledge, only a few works have investigated

the oxidation of phenolic pollutants by manganese oxides in situ in soils. For instance, studies have shown the oxidation of phenolic acids and dissolved organic matter by manganese oxides in soils, but these works focused on naturally occurring, non-contaminating compounds rather than phenolic-pollutant fate in the soil (Ding et al., 2022; Lehmann et al., 1987). In a study by Grebel et al. (2016), the oxidation of various phenolic contaminants was investigated using engineered MnO_2-coated sand columns, and their key conclusion underscores MnO_2 efficacy as an oxidizing agent for phenolic contaminants. However, to determine whether MnO_2 can be equally effective in natural soil environments, further investigation is required.

We aim to investigate the fate of phenolic pollutants, specifically in the context of oxidation processes in MnO_2-enriched soil. To achieve this, we will apply both classical methodologies and an advanced geoelectrical method recently introduced to soil science: spectral induced polarization (SIP) (Gao et al., 2019; Johansson et al., 2019; Kessouri et al., 2019; Mellage et al., 2022; Revil, 2012; Revil et al., 2021; Schwartz et al., 2012; Schwartz and Furman, 2012; Shefer et al., 2013; Vaudelet et al., 2011; Vinegar and Waxman, 1984; Zhang et al., 2012). This approach allows us not only to track the transformation of phenolic pollutants through oxidation by MnO_2 but also to monitor the broader impacts of this oxidation process on other elements within the soil environment.

SIP is a method where a low-frequency, time-dependent electrical field is applied, and the resultant potential is recorded. This technique captures both the conductive and capacitive characteristics of the surface, characterized by the in-phase (σ') and quadrature (σ'') conductivity, respectively, in a non-invasive way (Binley and Kemna, 2005; Binley and Slater, 2020; Reynolds, 2011). Quadrature and in-phase conductivity are associated with the interfacial chemistry of the grain surface and grain size, while in-phase conductivity is also related to pore water electrolyte conductivity (Ben Moshe and Furman, 2022). The σ'' is frequency dependent and is related to polarization processes at the electric double layer (EDL), and, indeed, Vinegar and Waxman (1984) proposed a linear relationship between the soil cation exchange capacity (CEC) and the σ''. Additionally, studies on the impact of organic contaminants on the low-frequency complex conductivity of soils and porous materials demonstrated the ability of the SIP method to detect and monitor organic contaminants within the subsurface (Kirmizakis et al., 2020; Mellage et al., 2018, 2022; Revil, 2012; Schwartz et al., 2020; Schwartz and Furman, 2012, 2015; Vaudelet et al., 2011).

This study aims to thoroughly explore the behavior of hydroquinone, a model phenolic molecule with a well-known mechanism of oxidation by means of Mn oxides, in MnO_2-enriched sandy soil (Mn-sandy soil). To achieve this, we employed an array of methods, including electric measurements of the soil profile, crystallographic and microscopic examination of the soil minerals, and chemical analysis of the soil solution. We hypothesized that integrating electrical measurements, soil solution analysis, and soil surface examinations would enable us to reach a unique understanding of the oxidation process in the soil and would provide insights into the resulting chemical mechanisms in the soil environment.

2 Materials and methods

In this study, we investigated the oxidation of hydroquinone by MnO_2 in sandy soil column experiments. The experiments were conducted using sandy soil and MnO_2-enriched sandy soil (Mn-sandy soil) to observe the behavior of hydroquinone and its oxidation product, benzoquinone. During the experiments, we employed SIP measurements to study the electrical characteristics of the soil as the oxidation process occurred. We analyzed the samples for hydroquinone and benzoquinone concentrations using high-performance liquid chromatography (HPLC) and measured ion concentrations and composition by means of coupled plasma atomic emission spectroscopy (ICP-AES), pH, and electrical conductivity (EC). Additionally, we conducted scanning electron microscopy (SEM), energy-dispersive X-ray spectroscopy (EDS), and X-ray diffraction (XRD) analyses to observe any changes in soil morphology and mineralogy before and after the introduction of hydroquinone into the soil.

Hydroquinone (99 % purity), benzoquinone (99 % purity), acetonitrile (HPLC grade), and calcium chloride were purchased from Sigma-Aldrich. Potassium permanganate and hydrochloride acid 32 % were purchased from Mercury LTD. Sandy soil with 97 % sand and 3 % silt (measured using PARIO, METER Group, Germany) contains 4 % $CaCO_3$ and 2.5 % organic matter.

2.1 MnO_2 preparation

MnO_2 was synthesized following the procedure of McKenzie (1971). In brief, concentrated HCl was added dropwise to a boiling solution of potassium permanganate to form a dark-purple precipitate of δ–MnO_2. After synthesis, the suspension was centrifuged (15 200 g, 15 min), and the supernatant was decanted and replaced with double-deionized water. The procedure was repeated until the supernatant was colorless; then the slurry was oven-dried overnight at 35 °C and freeze-dried.

2.2 Spectral induced polarization measurements

In the SIP method, a low-frequency (typically 0.01 Hz to 10 kHz) oscillating current $I(A)$ is applied through two electrodes on a porous medium, and electrical potential $U(V)$ is measured by two other electrodes. Using Ohm's law, the complex admittance of the medium $Y^* = I/U(S)$ is obtained. The complex conductivity is related to the admittance through the geometric factor G (m^{-1}) such that $\sigma^* = G \cdot Y^*$.

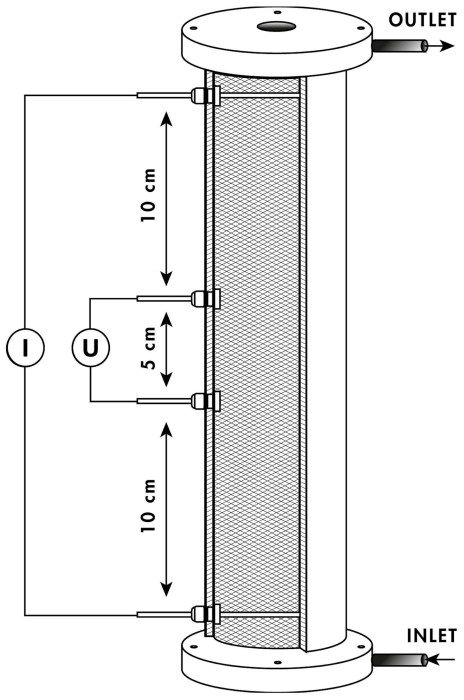

Figure 1. Scheme of experimental SIP column: inlet solution is injected in through the bottom, and the outlet is collected in fractions. The current (I) is injected between the top and the bottom electrodes, and the SIP signal is measured between the potential electrodes (U).

The complex conductivity signal can be expressed as $\sigma^* = \sigma' + i\sigma'' = |\sigma^*|e^{i\varphi}$, where σ' ($S\,m^{-1}$) is the in-phase conductivity (also referred to as the real conductivity), associated with energy dissipation processes; σ'' ($S\,m^{-1}$) is the quadrature conductivity (also referred to as the imaginary conductivity), related to energy storage processes (Vinegar and Waxman, 1984); and φ (rad) is the phase shift.

The SIP signal was measured using the PSIP impedance spectrometer (Ontash & Ermac Inc., NJ, USA) in polyvinyl chloride (3 cm diameter, 30 cm long) columns equipped with four brass electrodes, 6 mm in diameter, for both current injection and potential measurement (Fig. 1). The current electrodes were 8 cm long, and they crossed the entire sample, while the potential electrodes were 5 cm long, and they were retraced in their respective holes to prevent electrode polarization (as suggested by Cassiani et al., 2009, and Schwartz and Furman, 2012). Electrical contact between the potential electrodes and the sample was ensured through the electrolyte. The geometric factor (G) was determined by measuring the admittance of a series of electrolytes with different electrical conductivities.

2.3 Column experiments

Breakthrough experiments were conducted to study the behavior of hydroquinone and benzoquinone in sandy soil and Mn-sandy soil in an unbuffered environment. Two sets of experiments were performed using triplicate columns for each treatment: untreated sandy soil and Mn-sandy soil, which was prepared by mixing sandy soil with 5 % w/w MnO_2. Air-dried soil was mixed with 10 % w/w of $CaCl_2$ 5 mM solution as the saturating liquid. This soil was then packed in the columns in approximately 100 mL increments and gently compressed after each addition. Based on an assumed particle density of 2.65 g cm^{-3} (Warrick, 2002), the average porosity of the sandy soil and Mn-sandy soil samples was 0.4 and 0.44 ± 0.02, respectively.

After packing, the columns were placed vertically, and a 5 mM $CaCl_2$ solution was introduced from the bottom to wash away excess salt, ensuring saturated flow at a constant flow rate of 1 mL min^{-1} using a peristaltic pump (Masterflex L/S series, Cole-Parmer Inc., IL, USA). The soil was washed with $CaCl_2$ until equilibrium was reached between the inlet and outlet solutions (EC = 900 µS cm^{-1}). Upon reaching equilibrium, the inlet solution was replaced either by a mixed solution of hydroquinone and benzoquinone (0.1 M each in $CaCl_2$ 5 mM solution) for the sand-only columns or by a hydroquinone-only solution (0.1 M in $CaCl_2$ 5 mM solution) for the Mn-sandy soil columns. The mixed solution was used for the sand-only columns to ensure that no interactions occurred with benzoquinone, while the primary purpose was to follow the hydroquinone oxidation. Both solutions passed through their respective columns for four or eight pore volumes (PVs), respectively, until mass balance was achieved. Both solutions were left unbuffered and unpurged to better represent natural conditions.

Throughout the experiments, continuous SIP measurements were taken, and at 20 min intervals, 2 mL samples of the outlet solution were collected and immediately filtered using a 0.22 µm reverse cellulose membrane filter syringe for further analysis. The collected outflow was analyzed to determine (1) hydroquinone and benzoquinone concentrations using HPLC (Waters 600, Waters, Milford, MA), equipped with a diode-array detector. The HPLC column was an XBridge Phenyl 3.5 µm 4.6 × 150 mm, with a flow rate of 1 mL min^{-1}, and the column temperature was set to 25 °C. Hydroquinone and benzoquinone were monitored at wavelengths of 222 nm and 246 nm, respectively. The mobile phase consisted of acetonitrile and double-distilled water (DDW). The phase gradient started at 5 % acetonitrile for 0–3 min, was linearly increased to 40 % for 3–10 min, and then was increased again to 95 % over 10–11 min. Acetonitrile was maintained at 95 % over 11–12 min, was decreased back to 5 % over 12–13 min, and then was maintained at 5 % for 13–16 min. We also sought to determine (2) Ca^{2+} and soluble Mn concentration in the effluent by means of ICP-

AES (SPECTRO ARCOS Ltd., Germany) and (3) pH and EC values.

2.4 Colloid surface analysis by SEM-EDS and XRD

Sandy soil, MnO_2, and Mn-sandy soil morphology were observed before and after the introduction of hydroquinone by means of SEM (JEOL IT100, low-vacuum mode). All samples were oven-dried at 40 °C and thinly ground before analysis and were mounted on 30 mm round SEM aluminum stubs using adhesive carbon tape. Secondary electron images were taken using the following operating conditions: 20 keV, 9 mm working distance (WD), and × 350 magnification for all samples. For each soil, 10 images were obtained and scanned for calcium, manganese, and silica semi-quantitative percentages using EDS. The concentration of the elements in the Mn-sandy soil samples was corrected to the relative addition of Mn to the system. The effect of hydroquinone oxidation on Ca and Mn content in the soil was assessed using a non-parametric comparison for each pair using the Wilcoxon method. The statistical analysis was carried out by JMP®, version 16, SAS Institute Inc.

The mineralogy of the soil and the change in MnO_2 mineralogy pre- and post-oxidation were also evaluated by means of XRD. Soil samples were ground and loaded into an XRD sample holder by front loading followed by razor blade leveling. XRD patterns were acquired in Bragg–Brentano geometry using a PANalytical X'Pert diffractometer with CuKα radiation operated at 45 kV and 40 mA. The samples were scanned from 5 to 70° 2θ at a step size of 0.013° 2θ using a PIXcel detector in continuous-scanning-line (1D) mode with an active length of 3.35°. Mineral phase identification was performed using HighScore Plus® software based on the ICSD database.

3 Results and discussion

3.1 Hydroquinone and benzoquinone fate in sandy soils – breakthrough curves

Figure 2 illustrates the oxidation–reduction process (Fig. 2a) and breakthrough curves of hydroquinone and benzoquinone in sandy soil (Fig. 2b) and Mn-sandy soil (Fig. 2c) columns. Hydroquinone undergoes oxidation, involving the transfer of protons and electrons, to form benzoquinone (Fig. 2a). In the control sandy soil columns (Fig. 2b), both hydroquinone and benzoquinone displayed characteristic symmetric sigmoidal breakthrough curves, typical of inert substances that do not undergo adsorption or oxidation in the soil, with breakthrough occurring at approximately 1 pore volume (PV). This suggests that there was negligible adsorption or chemical transformation of these compounds in the sandy soil, allowing them to pass through the column relatively unimpeded.

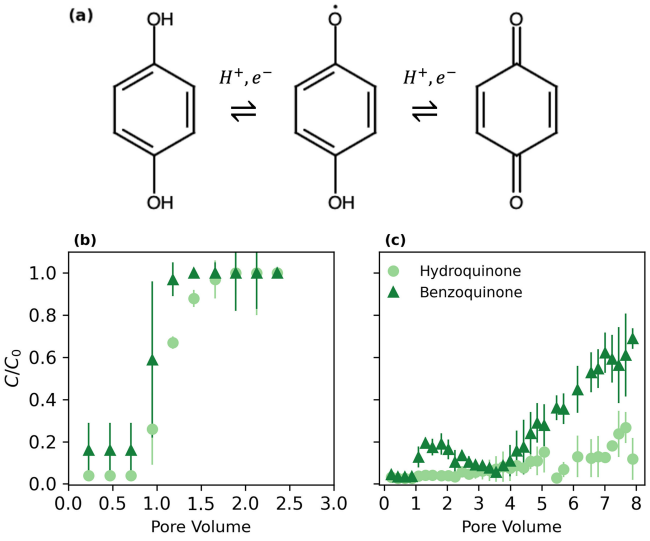

Figure 2. **(a)** Oxidation–reduction reactions of hydroquinone and benzoquinone. Relative concentrations of hydroquinone (0.1 M initial) and benzoquinone (0.1 M) in **(b)** sandy soil and **(c)** Mn-sandy soil columns.

Benzoquinone deviations likely occur due to measurement errors and may also be influenced by the reduction of benzoquinone under the natural, unbuffered conditions of the system used for these experiments.

In contrast, the breakthrough curves in the Mn-sandy soil columns (Fig. 2c) demonstrate different behavior. Benzoquinone showed an initial breakthrough at around 4 PVs, reaching a relative concentration (C/C_0) of about 0.2, and continued to increase gradually. Hydroquinone, however, exhibited a significantly delayed breakthrough, occurring at approximately 7 PVs, with a relative concentration of 0.7. The moderate slopes of these breakthrough curves compared to the steep slopes observed in the sandy soil columns indicate that hydroquinone undergoes oxidation in the presence of MnO_2, forming benzoquinone. This oxidation process is responsible for the delayed and more gradual breakthrough of hydroquinone, highlighting the reactive nature of the Mn-sandy soil in altering the transport and fate of these pollutants (Buamah et al., 2009).

3.2 SIP and soil solution chemistry monitoring

Sandy soil (control) and Mn-sandy soil columns were saturated with background solution (5 mM $CaCl_2$), and their SIP signatures were recorded upon reaching equilibrium before the introduction of the pollutant (Fig. 3). The quadrature conductivity (σ'') (associated with surface polarization) of the sandy soil exhibited classical spectra for the frequency-dependent polarization of porous media, with a peak at around 0.5 Hz (Fig. 3b). Compared to the sandy soil, σ'' of Mn-sandy soil increased by $\sim$ 40 %, most likely due to the contribution of the high CEC of MnO_2 (Händel et al., 2013;

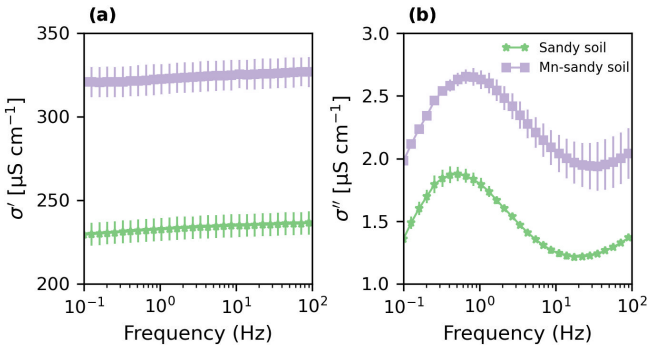

Figure 3. In-phase (σ') **(a)** and quadrature (σ'') **(b)** conductivity of sandy and Mn-sandy soils (5 % w/w).

McKenzie, 1971; Post, 1999). Similarly, the in-phase conductivity σ' was also higher ($\sim$ 40 %) than that of the sandy soil (Fig. 3a), most probably due to the contribution of MnO_2 to the surface conductivity of the media (recall that the EC of the soil solution was kept constant between the treatments).

Upon the addition of hydroquinone, the control columns demonstrated no change in both σ'' and σ' throughout the experiment (Fig. 4a, b). This was accompanied by negligible concentrations of benzoquinone and manganese, while the Ca^{2+} concentration remained constant at 5 mM in the effluent. Additionally, the EC remained constant at 1 mS m^{-1} $\pm$ 0.3, and the pH values were steady at 9$\pm$ 0.2 (Fig. 5a, b). These results indicate that there was neither adsorption nor oxidation of hydroquinone in the control columns, as also demonstrated by the breakthrough curves (Fig. 2a).

Hydroquinone flows through Mn-sandy soil columns induced a constant decrease in σ'', as expected, due to oxidation processes in the system, resulting in a reduction in oxidizing and polarizing surfaces (Fig. 4c, e). On the other hand, the σ' increased up to $\sim$4 PVs and then decreased (Fig. 4d, f). The maximum σ' value reached following $\sim$4 PVs corresponded to peaks in EC and pH values, as well as to the Ca^{2+} concentration in the effluents (Fig. 5c, d). The pH value and EC dramatically increased from 8.82 ($\pm$ 0.25) and 1.7 mS m^{-1} ($\pm$ 0.4) to 10.8 ($\pm$ 0.1) and 4.53 mS m^{-1} ($\pm$ 0.03), respectively (Fig. 5c). Simultaneously, the Ca^{2+} concentrations increased noticeably (from 0.1 to 25 mM), while the manganese concentrations increased only slightly (from below the detection limit to 0.1 mM) (Fig. 5d). Indeed, σ' is related to the bulk solution properties; i.e., an increase in ion concentration, mainly Ca^{2+}, will result in an increase in σ'. Notably, all maxima for Ca^{2+}, EC, σ', and pH corresponded to hydroquinone oxidation, as shown by benzoquinone breakthrough (Fig. 2b).

Since these trends are not observed in the control sandy soil columns (with hydroquinone flow but without MnO_2), we suggest that hydroquinone oxidation by MnO_2 surfaces initiated a cascade of reactions, with the first being (i) a local increase in proton concentration due to hydroquinone deprotonation decreasing the local pH (Rudolph et al., 2013). At this stage, two reactions, which require protons, may take place simultaneously but at different rates: (iia) calcite dissolution (made evident by the Ca^{2+}, EC, σ', and pH measurements) and (iib) MnO_2 reduction and dissolution to $Mn^{2+/3+}$ (Fukuzumi et al., 1975; McBride, 1987; Remucal and Ginder-Vogel, 2014; Stone and Ulrich, 1989), evidenced by benzoquinone breakthrough. The kinetics of calcite acid dissolution are at least 8 orders of magnitude higher than those of oxide acid dissolution (Palandri and Kharaka, 2004); i.e., the protons are consumed faster by the calcite than by the oxidation reaction. (iii) The oxidation processes diminish due to adsorption or precipitation of $Mn^{2+/3+}$ as amorphous Mn oxides on the birnessite (MnO_2) surface (Ding et al., 2022; Remucal and Ginder-Vogel, 2014; Stone and Ulrich, 1989), also supported by the very low manganese concentrations being eluted (0.1 mM). (iv) Calcite dissolution is suppressed, resulting in a decrease in Ca^{2+}, EC, σ', and pH. Indeed, the decrease in σ'' reflects the reduction in $CaCO_3$ content in the soil (Izumoto et al., 2020; Wu et al., 2010) and may also correlate with a reduction in active MnO_2 surfaces. To further support this suggested cascade of reactions, we tested the precipitation of $Mn^{+2/+3}$ as amorphous Mn oxides.

3.3 Soil mineral characterization

To further test MnO_2 dissolution and $Mn^{2+/3+}$ precipitation, we characterized the soil samples before and after hydroquinone oxidation using XRD (Fig. 6a). The sandy soil was found to be composed mainly of quartz, feldspar, and calcite. X-ray diffraction analysis confirmed that the Mn-sandy soil initially contained approximately 5 % MnO_2. After hydroquinone oxidation, the MnO_2 content was reduced to $\sim$ 1 %, indicating that Mn^{4+} was most likely reduced to $Mn^{2+/3+}$. These reduced manganese ions likely precipitated as amorphous Mn oxides or were adsorbed onto the MnO_2 surface, which would not be detected by XRD. This conclusion is further supported by the very low concentration of $Mn^{2+/3+}$ being eluted from the columns (Fig. 5b, d).

Finally, SEM images coupled with EDS analysis of the samples (two replicates, 10 images per sample) confirm the reduction in Ca content post-oxidation, while the Mn content remains constant in both samples (Fig. 6b). SEM images vividly depict the morphology of pure MnO_2 (Fig. 6c), quartz, and $CaCO_3$ deposits in the sandy soil samples (Fig. 6d). In the Mn-sandy soil samples, MnO_2 is also notably present (Fig. 6e). Comparisons of post-oxidation samples to pre-oxidation samples showed no significant visual changes (Fig. 6e, f).

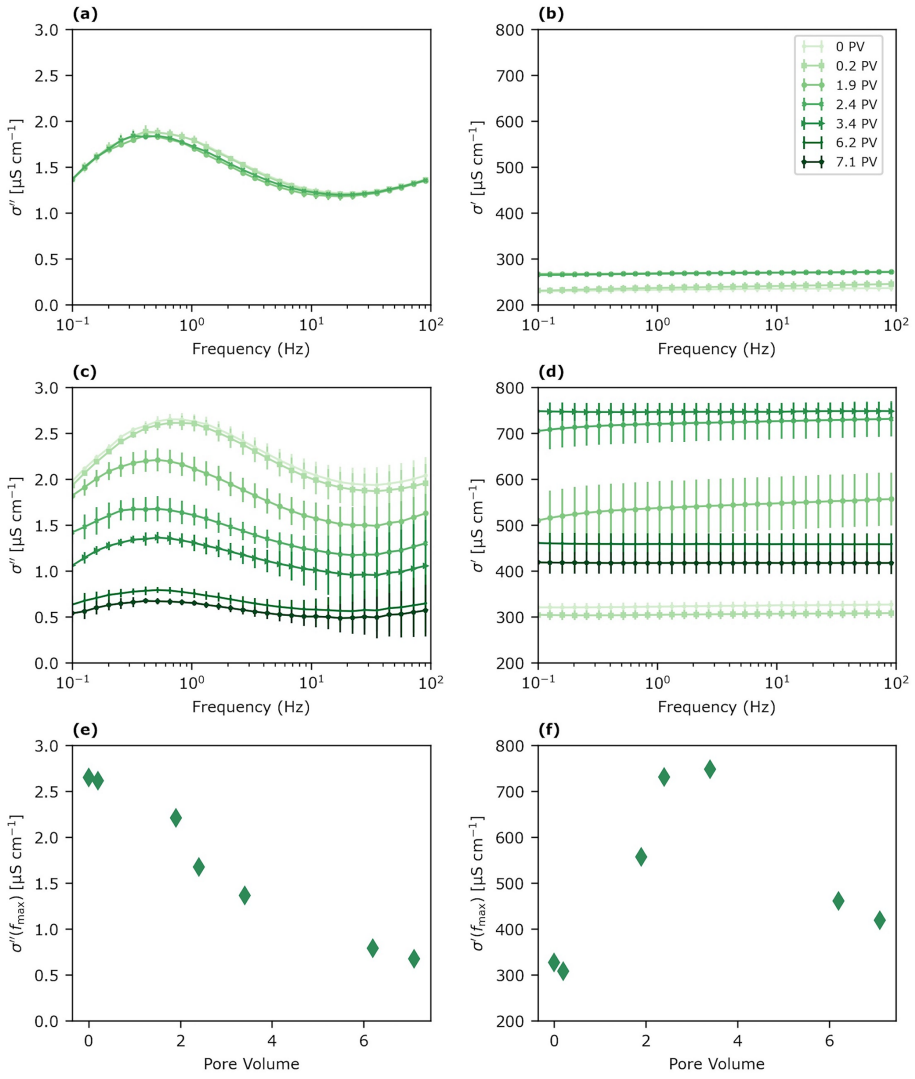

Figure 4. Quadrature (σ'') and in-phase (σ') conductivity of sandy soils **(a, b)** and Mn-sandy soils **(c, d)** during hydroquinone oxidation. σ'' **(e)** and σ' **(f)** at the peak frequency of Mn-sandy soil.

4 Conclusions

We explored the oxidation mechanism of hydroquinone in Mn-sandy soil by applying a combination of methods, including electrical measurements (SIP), crystallographic analysis (XRD), microscopic examination (SEM-EDS) of soil minerals, and chemical assessments of the soil solution (HPLC, ICP, pH, EC, etc.). Integrating results from these different methods provided insights into subsequent reactions such as mineral dissolution, chemical precipitation, and leaching.

Our findings suggest that hydroquinone oxidation by MnO_2 surfaces to benzoquinone initiated a cascade of reactions, starting with local alterations to pH levels. These triggers increased $CaCO_3$ dissolution, while, simultaneously, MnO_2 reduction resulted in its dissolution to $Mn^{2+/3+}$ and its adsorption or precipitation as amorphous Mn oxides on the MnO_2 surface. These results were supported by both chemical and electrical measurements. $CaCO_3$ dissolution was identified by a reduction in Ca by means of SEM-EDS analysis and by the SIP signature, showing a consistent decline in σ'' due to a reduction in polarized surfaces. The changes in Ca^{2+} concentrations in the effluent were monitored by ICP and were reflected in the alternating σ' signature. The effluent contained only a minimal Mn concentration. XRD and SEM-EDS analysis results demonstrated a reduction in MnO_2 content and constant Mn content, respectively.

These combined findings support the precipitation of $Mn^{2+/3+}$ as amorphous Mn oxides and MnO_2 surface passivation, most likely also contributing to the consistent decrease in σ''. This study has provided valuable insights into

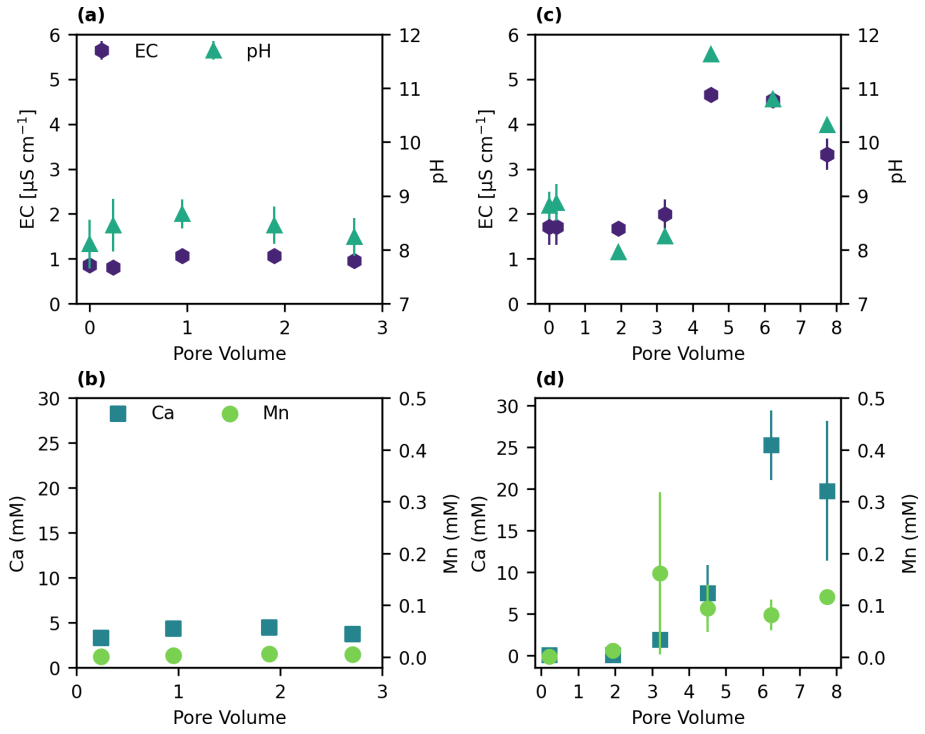

Figure 5. Effluent measurements of EC, pH, Ca^{2+}, and Mn concentrations in **(a, b)** sandy soil and **(c, d)** Mn-sandy soil.

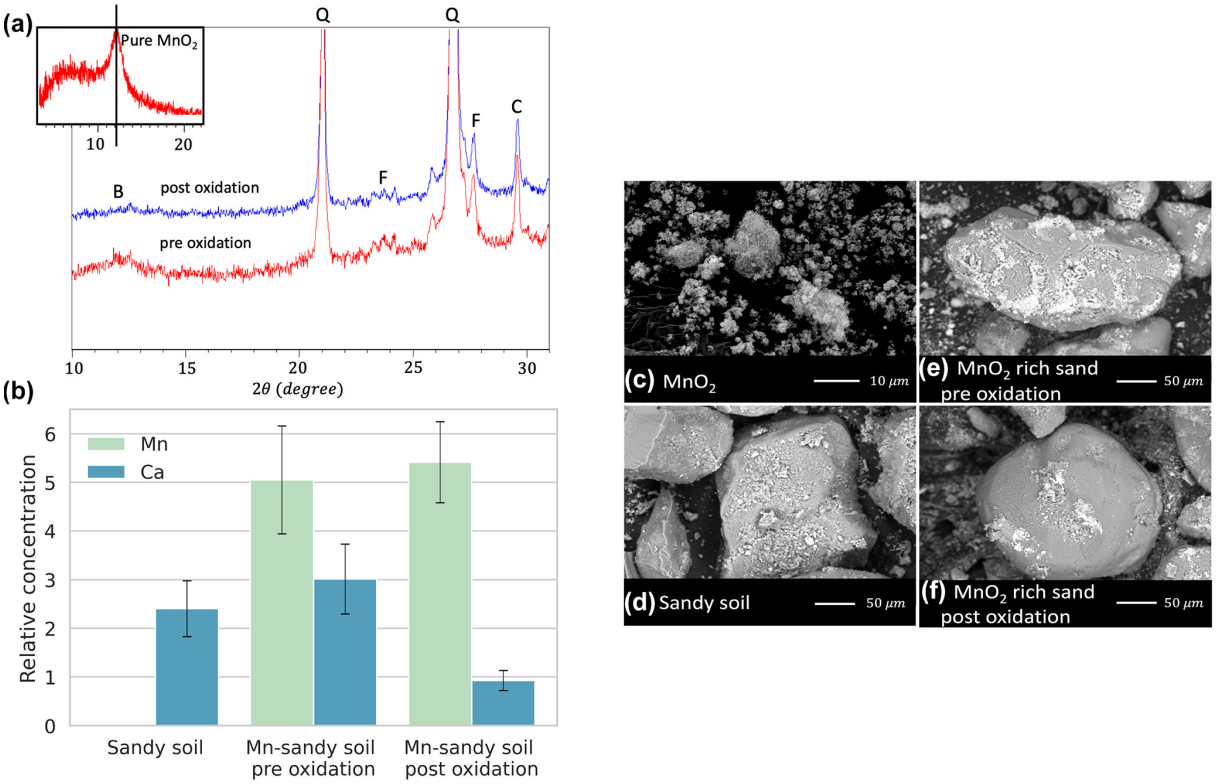

Figure 6. **(a)** X-ray diffraction full characterization curve of Mn-sandy soil pre- and post-oxidation, along with MnO_2 inset. B, Q, F, and C represent the peaks of birnessite, quartz, feldspar, and calcite. **(b)** Ca and Mn relative concentrations determined by EDS analysis. Scanning electron micrographs of **(c)** MnO_2, **(d)** sandy soil, **(e)** MnO_2-rich sandy soil, and **(f)** MnO_2-rich sandy soil post-oxidation.

the sensitivity of SIP signatures to changes in soil properties due to oxidation processes within the soil. Future research should include the dynamic role of microbial activity in altering soil redox conditions, leading to MnO_2 reduction or $CaCO_3$ dissolution. Furthermore, deeper exploration of the implications of soil structure changes resulting from $CaCO_3$ dissolution and precipitation for the fate of pollutants in the subsurface is necessary, including a consideration of diverse pollutant groups, organic matter, etc. In natural environments and at the field scale, the complexities will require further investigation, with potential for the formulation of effective environmental remediation strategies.

Code and data availability. All data sets are available from the authors upon request.

Author contributions. SSA, YGM, and NS designed the study. SSA processed and interpreted the data, with contributions from all of the co-authors. SSA wrote the paper, and YGM and NS reviewed the paper.

Competing interests. The contact author has declared that none of the authors has any competing interests.

Disclaimer. Publisher's note: Copernicus Publications remains neutral with regard to jurisdictional claims made in the text, published maps, institutional affiliations, or any other geographical representation in this paper. While Copernicus Publications makes every effort to include appropriate place names, the final responsibility lies with the authors.

Financial support. This research has been supported by the Isaac Dreyfus-Bernheim Foundation, the Ministry of Science and Technology of Israel (grant no. 80689), and Hebrew University of Jerusalem internal funding (grant no. 54731).

Review statement. This paper was edited by Olivier Evrard and reviewed by Damien Jougnot and one anonymous referee.

References

Ahmed, A. A., Thiele-Bruhn, S., Aziz, S. G., Hilal, R. H., Elroby, S. A., Al-Youbi, A. O., Leinweber, P., and Kühn, O.: Interaction of polar and nonpolar organic pollutants with soil organic matter: Sorption experiments and molecular dynamics simulation, Sci. Total Environ., 508, 276–287, https://doi.org/10.1016/J.SCITOTENV.2014.11.087, 2015.

Ben Moshe, S. and Furman, A.: Real-time monitoring of organic contaminant adsorption in activated carbon filters using spectral induced polarization, Water Res., 212, 118103, https://doi.org/10.1016/j.watres.2022.118103, 2022.

Binley, A. and Kemna, A.: DC Resistivity and Induced Polarization Methods, Hydrogeophysics, 50, 129–156, https://doi.org/10.1007/1-4020-3102-5_5, 2005.

Binley, A. and Slater, L.: Resistivity and induced polarization: Theory and applications to the near-surface earth, Cambridge University Press, ISBN: 1-108-69459-4, 2020.

Buamah, R., Petrusevski, B., and Schippers, J. C.: Oxidation of adsorbed ferrous iron: kinetics and influence of process conditions, Water Sci. Technol., 60, 2353–2363, https://doi.org/10.2166/wst.2009.597, 2009.

Cassiani, G., Kemna, A., Villa, A., and Zimmermann, E.: Spectral induced polarization for the characterization of free-phase hydrocarbon contamination of sediments with low clay content, Surf. Geophys., 7, 547–562, https://doi.org/10.3997/1873-0604.2009028, 2009.

Chien, S. W. C., Chen, H. L., Wang, M. C., and Seshaiah, K.: Oxidative degradation and associated mineralization of catechol, hydroquinone and resorcinol catalyzed by birnessite, Chemosphere, 74, 1125–1133, https://doi.org/10.1016/j.chemosphere.2008.10.007, 2009.

Davì, M. L. and Gnudi, F.: Phenolic compounds in surface water, Water Res., 33, 3213–3219, https://doi.org/10.1016/S0043-1354(99)00027-5, 1999.

Delgado-Moreno, L., Bazhari, S., Gasco, G., Méndez, A., Azzouzi, M. E., and Romero, E.: New insights into the efficient removal of emerging contaminants by biochars and hydrochars derived from olive oil wastes, Sci. Total Environ., 752, 141838, https://doi.org/10.1016/J.SCITOTENV.2020.141838, 2021.

Ding, Z., Ding, Y., Liu, F., Yang, J., Li, R., Dang, Z., and Shi, Z.: Coupled Sorption and Oxidation of Soil Dissolved Organic Matter on Manganese Oxides: Nano/Sub-nanoscale Distribution and Molecular Transformation, Environ. Sci. Technol., 56, 2783–2793, https://doi.org/10.1021/acs.est.1c07520, 2022.

Farhan Hanafi, M. and Sapawe, N.: A review on the water problem associate with organic pollutants derived from phenol, methyl orange, and remazol brilliant blue dyes, Mater. Today Proc., 31, A141–A150, https://doi.org/10.1016/j.matpr.2021.01.258, 2020.

Fukuzumi, S.-I., Ono, Y., and Keii, T.: ESR Studies on the Formation of p-Benzosemiquinone Anions over Manganese Dioxide, Int. J. Chem. Kinet., 7, 535–546, https://doi.org/10.1002/kin.550070405, 1975.

Gao, Z., Haegel, F.-H., Esser, O., Zimmermann, E., Vereecken, H., and Huisman, J. A.: Spectral Induced Polarization of Biochar in Variably Saturated Soil, Vadose Zone J., 18, 180213, https://doi.org/10.2136/vzj2018.12.0213, 2019.

Grebel, J. E., Charbonnet, J. A., and Sedlak, D. L.: Oxidation of organic contaminants by manganese oxide geomedia for passive urban stormwater treatment systems, Water Res., 88, 481–491, https://doi.org/10.1016/j.watres.2015.10.019, 2016.

Gusain, R., Gupta, K., Joshi, P., and Khatri, O. P.: Adsorptive removal and photocatalytic degradation of organic pollutants using metal oxides and their composites: A comprehensive review, Adv. Colloid Interface Sci., 272, 102009, https://doi.org/10.1016/j.cis.2019.102009, 2019.

Händel, M., Rennert, T., and Totsche, K. U.: A simple method to synthesize birnessite at ambient pres-

sure and temperature, Geoderma, 193/194, 117–121, https://doi.org/10.1016/j.geoderma.2012.09.002, 2013.

Izumoto, S., Huisman, J. A., Wu, Y., and Vereecken, H.: Effect of solute concentration on the spectral induced polarization response of calcite precipitation, Geophys. J. Int., 220, 1187–1196, https://doi.org/10.1093/gji/ggz515, 2020.

Johansson, S., Rossi, M., Hall, S. A., Sparrenbom, C., Hagerberg, D., Tudisco, E., Rosqvist, H., and Dahlin, T.: Combining spectral induced polarization with X-ray tomography to investigate the importance of DNAPL geometry in sand samples, Geophysics, 84, E173–E188, https://doi.org/10.1190/geo2018-0108.1, 2019.

Kang, S. H. and Choi, W.: Oxidative Degradation of Organic Compounds Using Zero-Valent Iron in the Presence of Natural Organic Matter Serving as an Electron Shuttle, Environ. Sci. Technol., 43, 878–883, https://doi.org/10.1021/ES801705F, 2008.

Kessouri, P., Furman, A., Huisman, J. A., Martin, T., Mellage, A., Ntarlagiannis, D., Bücker, M., Ehosioke, S., Fernandez, P., Flores-Orozco, A., Kemna, A., Nguyen, F., Pilawski, T., Saneiyan, S., Schmutz, M., Schwartz, N., Weigand, M., Wu, Y., Zhang, C., and Placencia-Gomez, E.: Induced polarization applied to biogeophysics: recent advances and future prospects, Surf. Geophys., 17, 595–621, https://doi.org/10.1002/nsg.12072, 2019.

Kirmizakis, P., Kalderis, D., Ntarlagiannis, D., and Soupios, P.: Preliminary assessment on the application of biochar and spectral-induced polarization for wastewater treatment, Surf. Geophys., 18, 109–122, https://doi.org/10.1002/nsg.12076, 2020.

Lambert, J. F.: Organic pollutant adsorption on clay minerals, Dev. Clay Sci., 9, 195–253, https://doi.org/10.1016/B978-0-08-102432-4.00007-X, 2018.

Lehmann, R. G., Cheng, H. H., and Harsh, J. B.: Oxidation of Phenolic Acids by Soil Iron and Manganese Oxides, Soil Sci. Soc. Am. J., 51, 352–356, https://doi.org/10.2136/sssaj1987.03615995005100020017x, 1987.

Liao, X., Zhang, C., Nan, C., Lv, Y., Fan, Z., and Hu, L.: Phenol driven changes onto MnO_2 surface for efficient removal of methyl parathion: The role of adsorption, Chemosphere, 269, 128695, https://doi.org/10.1016/j.chemosphere.2020.128695, 2021.

Liu, M. M., Cao, X. H., Tan, W. F., Feng, X. H., Qiu, G. H., Chen, X. H., and Liu, F.: Structural controls on the catalytic polymerization of hydroquinone by birnessites, Clays Clay Miner., 59, 525–537, https://doi.org/10.1346/CCMN.2011.0590510, 2011.

Loffredo, E. and Senesi, N.: Fate of anthropogenic organic pollutants in soils with emphasis on adsorption/desorption processes of endocrine disruptor compounds, Pure Appl. Chem., 78, 947–961, 2006.

McBride, M. B.: Adsorption and Oxidation of Phenolic Compounds by Iron and Manganese Oxides, Soil Sci. Soc. Am. J., 51, 1466–1472, https://doi.org/10.2136/sssaj1987.03615995005100060012x, 1987.

McKenzie, R. M.: The synthesis of birnessite, cryptomelane, and some other oxides and hydroxides of manganese, Mineral. Mag., 38, 493–502, https://doi.org/10.1180/MINMAG.1971.038.296.12, 1971.

Mellage, A., Holmes, A. B., Linley, S., Vallée, L., Rezanezhad, F., Thomson, N., Gu, F., and Cappellen, P. V.: Sensing Coated Iron-Oxide Nanoparticles with Spectral Induced Polarization (SIP): Experiments in Natural Sand Packed Flow-Through Columns, Environ. Sci. Technol., 52, 14256–14265, 2018.

Mellage, A., Zakai, G., Efrati, B., Pagel, H., and Schwartz, N.: Paraquat sorption- and organic matter-induced modifications of soil spectral induced polarization (SIP) signals, Geophys. J. Int., 229, 1422–1433, https://doi.org/10.1093/GJI/GGAB531, 2022.

Murray, J. W.: The surface chemistry of hydrous manganese dioxide, J. Colloid Interface Sci., 46, 357–371, https://doi.org/10.1016/0021-9797(74)90045-9, 1974.

Palandri, J. L. and Kharaka, Y. K.: A compilation of rate parameters of water-mineral interaction kinetics for application to geochemical modeling, Report, U.S. Geological Survey, https://doi.org/10.3133/ofr20041068, 2004.

Post, J. E.: Manganese oxide minerals: Crystal structures and economic and environmental significance, P. Natl. Acad. Sci. USA, 96, 3447–3454, 1999.

Remucal, C. K. and Ginder-Vogel, M.: A critical review of the reactivity of manganese oxides with organic contaminants, Environ. Sci. Process. Impacts, 16, 1247–1266, https://doi.org/10.1039/C3EM00703K, 2014.

Revil, A.: Spectral induced polarization of shaly sands: Influence of the electrical double layer, Water Resour. Res., 48, W02517, https://doi.org/10.1029/2011WR011260, 2012.

Revil, A., Schmutz, M., Abdulsamad, F., Balde, A., Beck, C., Ghorbani, A., and Hubbard, S. S.: Field-scale estimation of soil properties from spectral induced polarization tomography, Geoderma, 403, 115380, https://doi.org/10.1016/j.geoderma.2021.115380, 2021.

Reynolds, J. M.: An Introduction to Applied and Environmental Geophysics, 2nd Edn., John Wiley & Sons, England, 373–398, 2011.

Rudolph, N., Voss, S., Moradi, A. B., Nagl, S., and Oswald, S. E.: Spatio-temporal mapping of local soil pH changes induced by roots of lupin and soft-rush, Plant Soil, 369, 669–680, https://doi.org/10.1007/s11104-013-1775-0, 2013.

Schwartz, N. and Furman, A.: Spectral induced polarization signature of soil contaminated by organic pollutant: Experiment and modeling, J. Geophys. Res.-Sol. Ea., 117, 10203, https://doi.org/10.1029/2012JB009543, 2012.

Schwartz, N. and Furman, A.: On the spectral induced polarization signature of soil organic matter, Geophys. J. Int., 200, 589–595, https://doi.org/10.1093/GJI/GGU410, 2015.

Schwartz, N., Huisman, J. A., and Furman, A.: The effect of NAPL on the electrical properties of unsaturated porous media, Geophys. J. Int., 188, 1007–1011, 2012.

Schwartz, N., Levy, L., Carmeli, B., and Radian, A.: Spectral induced polarization of clay-oxide hybrid particles, J. Colloid Interface Sci., 577, 173–180, https://doi.org/10.1016/J.JCIS.2020.05.029, 2020.

Shefer, I., Schwartz, N., and Furman, A.: The effect of free-phase NAPL on the spectral induced polarization signature of variably saturated soil, Water Resour. Res., 49, 6229–6237, https://doi.org/10.1002/WRCR.20502, 2013.

Shindo, H. and Huang, P. M.: Catalytic Effects of Manganese (IV), Iron(III), Aluminum, and Silicon Oxides on the Formation of Phenolic Polymers, Soil Sci. Soc. Am. J., 48, 927–934, https://doi.org/10.2136/sssaj1984.03615995004800040045x, 1984.

Stone, A. T. and Ulrich, H.-J.: Kinetics and Reaction Stoichiometry in the Reductive Dissolution of Manganese(IV) Dioxide and Co(Ill) Oxide by Hydroquinone, J. Colloid Interf. Sci., 132, 509–522, https://doi.org/10.1016/0021-9797(89)90265-8, 1989.

Sun, J., Mu, Q., Kimura, H., Murugadoss, V., He, M., Du, W., and Hou, C.: Oxidative degradation of phenols and substituted phenols in the water and atmosphere: a review, Adv. Compos. Hybrid Mater., 5, 627–640, https://doi.org/10.1007/s42114-022-00435-0, 2022.

Trainer, E. L., Ginder-Vogel, M., and Remucal, C. K.: Selective Reactivity and Oxidation of Dissolved Organic Matter by Manganese Oxides, Environ. Sci. Technol., 55, 12084–12094, https://doi.org/10.1021/acs.est.1c03972, 2021.

Vaudelet, P., Revil, A., Schmutz, M., Franceschi, M., and Bégassat, P.: Changes in induced polarization associated with the sorption of sodium, lead, and zinc on silica sands, J. Colloid Interface Sci., 360, 739–752, https://doi.org/10.1016/J.JCIS.2011.04.077, 2011.

Vinegar, H. J. and Waxman, M. H.: Induced polarization of shaly sands, Geophysics, 49, 1267–1287, https://doi.org/10.1190/1.1441755, 1984.

Warrick, A. W. (Ed.): Soil physics companion, CRC Press, Boca Raton, FL, 389 pp., https://doi.org/10.1201/9781420041651, 2002.

Wu, Y., Hubbard, S., Williams, K. H., and Ajo-Franklin, J.: On the complex conductivity signatures of calcite precipitation, J. Geophys. Res.-Biogeo., 115, G00G04, https://doi.org/10.1029/2009JG001129, 2010.

Zhang, C., Slater, L., Redden, G. D., Fujita, Y., Johnson, T. J., Johnson, T. C., and Fox, D. T.: Spectral Induced Polarization Signatures of Hydroxide Adsorption and Mineral Precipitation in Porous Media, Environ. Sci. Technol., 46, 4357–4364, https://doi.org/10.1021/es204404e, 2012.